



Breaking wave induced cross-shore tracer dispersion in the surf zone: Model results and scalings

Falk Feddersen¹

Received 8 November 2006; revised 23 May 2007; accepted 11 June 2007; published 15 September 2007.

[1] The dispersion of surf zone tracers including pollutants and bacteria is determined by many processes acting over a range of timescales and space scales. Breaking waves (bores) are clearly important to cross-shore tracer dispersion in the surf zone, but little is known about the dispersal effects of bores. Here, a simple model for bore induced cross-shore dispersion are developed based upon the diffusion equation with an eddy diffusivity that propagates with the bores. Depth-uniform tracer and bore-induced mixing along with alongshore uniformity are assumed. The bores are assumed well developed and the dispersion results are for a self-similar (constant wave height to water depth ratio) surf zone. Four nondimensional parameters are identified and solution space is explored. The tracer center of mass is approximately constant, and tracer width grows with the square root of time. Tracer distribution becomes initially skewed after the passage of the first bore but becomes symmetric after multiple bores have passed. The nondimensional tracer patch growth and dilution rates depend strongly upon the nondimensional phase speed and wave period. The simple model results are consistent with the a Boussinesq wave model where the breaking-wave eddy viscosity is used for the bore eddy diffusivity. The scaling of the dimensional parameters regarding the bore eddy diffusivity and the ranges of the nondimensional parameters are examined. Covariation of the nondimensional phase speed and wave period suggest that nondimensional tracer dispersion is largely cross-shore independent.

Citation: Feddersen, F. (2007), Breaking wave induced cross-shore tracer dispersion in the surf zone: Model results and scalings, *J. Geophys. Res.*, 112, C09012, doi:10.1029/2006JC004006.

1. Introduction

[2] Terrestrial runoff is the main source of urban coastal pollution [Schiff *et al.*, 2000]. Often draining directly onto the shoreline, runoff degrades surf zone water quality leading to beach closures [e.g., Boehm *et al.*, 2002], increases the health risks (e.g., diarrhea and upper respiratory illness) to ocean bathers [Haile *et al.*, 1999], and contains both elevated fecal bacteria levels and human viruses [Jiang and Chu, 2004]. The details of pollution transport, dispersal, and dilution in the surf zone and nearshore are not understood. An improved understanding requires that the physical mechanisms for transport and dispersion of a (passive and conservative) tracer are diagnosed.

[3] In a time-averaged sense, tracer is transported (advected) by the mean surf zone circulation including the mean alongshore current \bar{v} and offshore directed rip currents. Surf zone mean alongshore current \bar{v} often are well predicted by simple models balancing breaking-wave induced forcing with bottom stress [e.g., Thornton and Guza, 1986; Ruessink *et al.*, 2001]. In cases with a known source, the

direction (up or down coast) of surf zone pollutant transport can be predicted [Grant *et al.*, 2005] with simple \bar{v} models driven with incident waves and wind. Tracer also may be transported shoreward with the Stokes drift [e.g., Monismith and Fong, 2004] and seaward at depth in the undertow, both of which are typically weaker than the alongshore current. Overall though, the details of surf zone tracer transport require further investigation.

[4] Several physical mechanisms over a range of space scales and timescales disperse tracer horizontally in the surf zone. As discussed by Inman *et al.* [1971] and Bowen and Inman [1974], surf zone dispersion and mixing conceptually can be separated into two categories, dispersion due to breaking waves and large-scale (>surf zone width) dispersion due to the wave-driven circulation. The effective diffusivity due to these two mechanisms likely is quite different.

[5] On larger length scales (20–100 m) and timescales (many minutes), horizontal dispersion is driven by surf zone eddies, meanders, and transient rip currents [e.g., Allen *et al.*, 1996; Özkan-Haller and Li, 2003] associated with shear waves [Oltman-Shay *et al.*, 1992; Bowen and Holman, 1989] and possibly vertical vorticity induced by breaking waves with finite crest length [Peregrine, 1998; Johnson and Pattiaratchi, 2006; Spydell *et al.*, 2007]. On beaches with alongshore nonuniform bathymetry or waves, stationary rip currents and other circulation features [e.g., Inman *et al.*,

¹Integrative Oceanography Division, Scripps Institution of Oceanography, La Jolla, California, USA.

1971; *Slinn et al.*, 2000] may also disperse tracer on longer timescales. In addition, time-dependent variations in the Stokes drift of random waves can weakly disperse tracer patches that are large relative to the wavelength [*Herterich and Hasselmann*, 1982]. However, the dispersion expected by this mechanism was orders of magnitude smaller than observed with surf zone drifters [*Spydell et al.*, 2007].

[6] Over smaller space scales and timescales, cross-shore tracer dispersion is caused by breaking-wave generated turbulence. *Inman et al.* [1971] found that dye mixed rapidly (approximately 140 s) across the surf zone (of widths 70 m) due to the action of breaking waves. Qualitative surf zone observations (R. T. Guza and D. Clark, personal communication, 2006) clearly show that individual breaking waves (bores) each disperse tracer in the cross-shore. No theory exists for how breaking waves disperse tracer in the cross-shore.

[7] Surf zone bores do not disperse drifters as the drifters duck under bores [*Schmidt et al.*, 2003; *Spydell et al.*, 2007]. In addition, surf zone drifters generally span significant fraction of the water depth averaging over motions with scales shorter than the height of the drifter. Horizontal plates [*Schmidt et al.*, 2003] or parachutes [*Johnson and Pattiaratchi*, 2004] further dampen turbulent motions. Thus tracer and drifters will have different surf zone cross-shore dispersion rates, and drifters cannot be utilized to study breaking-wave induced cross-shore dispersion.

[8] Time-dependent Boussinesq wave models such as FUNWAVE [*Chen et al.*, 1999; *Kennedy et al.*, 2000] simulate wave breaking with an eddy viscosity term in the momentum equations, associated with the front face of steep (breaking) waves. This approach dissipates wave energy and reproduces observed wave height variation across the surf zone in the laboratory [*Kennedy et al.*, 2000] and field [*Chen et al.*, 2003]. Given the effectiveness of the eddy viscosity approach in the momentum equations, it is hypothesized to apply for tracer dispersion through an eddy diffusivity κ associated with the front face of a bore (breaking wave). This is the mechanism discussed by *Inman et al.* [1971] and is the approach taken here.

[9] The cross-shore dispersion of surf zone tracer due solely to bore (breaking-wave) induced mixing is studied with a simple model based on the diffusion equation that uses a propagating eddy diffusivity to represent the bore mixing (section 2). The depth-integrated model assumes vertically uniform tracer and bore-induced mixing. The nondimensional parameters governing the solutions are found and scalings for the nondimensional tracer moments are developed. The solutions for different nondimensional parameters are explored (section 3) by examining the integral moments of tracer dispersion (i.e., center-of-mass, tracer width, and skewness). The effect of a single bore on a tracer patch is initially examined, with the additional factors of multiple periodic bores and a sloping bathymetry considered subsequently. The principal results include the following: (1) The location of the tracer center of mass remains nearly constant. (2) The tracer patch width grows as $(\alpha t)^{1/2}$ (t is time) and α depends upon the nondimensional parameters. (3) A single bore results in a skewed tracer distribution but that multiple bores result in a more symmetric distribution.

[10] Cross-shore tracer dispersion is also modeled with a more complex Boussinesq wave model that includes wave breaking and also assumes vertically uniform tracer and bore-induced mixing (section 4). Scalings for the dimensional parameters governing the dispersion are verified and the nondimensional parameters range is found. The tracer dispersion moments from the Boussinesq model solutions and the simple model agree well. These results provide testable hypotheses regarding breaking-wave driven tracer dispersion that can be examined with future laboratory or field observations. Features of qualitative laboratory observations of surf zone tracer dispersion and potential drawbacks to the simple models and the eddy diffusivity mechanism associated with the bore are discussed in section 5. The results are summarized in section 6.

2. Simple Model

[11] An idealized simple model for bore-induced surf zone tracer dispersion based on the diffusion equation is developed. Surf zone tracer dispersion is assumed to result only from the eddy diffusivity on the front face of the bore (breaking wave). This is analogous to eddy viscosity representations for the effects of wave breaking [e.g., *Zelt*, 1991; *Kennedy et al.*, 2000] in the Boussinesq momentum equations and resembles the approach of *Inman et al.* [1971]. Other potential bore dispersion mechanisms such as wave rollers are not considered. The effect of orbital wave velocities is neglected, as are other surf zone dispersion processes (e.g., shear waves). The simple model applies only within a self-similar surf zone where bores are well developed and the wave height to water depth ratio is approximately constant. The simple model is developed in hierarchical components that build upon each other. Modeling the effect of a single bore on a tracer is described first. Next, the effect of multiple periodic bores is included in the model. Finally, depth variation, which affects bore phase speed and mixing intensity, is included.

2.1. Single Bore

[12] Alongshore (y) uniform conditions (i.e., $\partial_y = 0$) are assumed. The depth-average tracer concentration ϕ is assumed vertically uniform due to the strong vertical mixing in the surf zone. This assumption is discussed further in section 5. The evolution of depth-integrated tracer is given by a diffusion equation

$$\partial_t[h\phi] = \partial_x[\kappa h\partial_x\phi] \quad (1)$$

where t and x are time and cross-shore position ($x = 0$ is at the tracer patch initial center and positive onshore), respectively, h is the water depth, and κ is the breaking wave induced tracer eddy diffusivity. No flux boundary conditions ($\partial_x\phi = 0$) at the onshore and offshore boundaries (located at $x = \pm L_x$) are chosen.

[13] Initially, h is assumed constant, reducing (1) to the standard diffusion equation

$$\partial_t\phi = \partial_x[\kappa\partial_x\phi]. \quad (2)$$

The breaking wave induced eddy diffusivity κ propagates with the waves, $\kappa = \kappa(x - ct)$ where $c = \sqrt{gh}$ is the wave

phase speed. With constant h , c is also a constant. The form for the eddy diffusivity is chosen as

$$\kappa(x - ct) = \kappa_0 \exp \left[-\frac{(x - ct)^2}{2L_\kappa^2} \right] \quad (3)$$

where κ_0 sets the diffusion magnitude and L_κ is the length scale of the mixing region (the half-width of the bore).

[14] The variables are nondimensionalized with

$$x = L_\kappa \hat{x}, \quad t = \tau \hat{t}, \quad \kappa = \kappa_0 \hat{\kappa}, \quad \phi = \phi_0 \hat{\phi}$$

where \hat{x} , \hat{t} , $\hat{\kappa}$, $\hat{\phi}$ are the respective nondimensional variables, and ϕ_0 is the initial peak concentration. With the diffusive timescale $\tau = L_\kappa^2/\kappa_0$, (2) becomes

$$\partial_t \hat{\phi} = \partial_{\hat{x}} \left[\hat{\kappa} \partial_{\hat{x}} \hat{\phi} \right], \quad (4)$$

with the nondimensional diffusivity $\hat{\kappa}$,

$$\hat{\kappa} = \exp \left[-\frac{(x - ct)^2}{2L_\kappa^2} \right] = \exp \left[-\frac{1}{2} (\hat{x} - \hat{c}\hat{t})^2 \right] \quad (5)$$

where nondimensional phase speed $\hat{c} = c\tau/L_\kappa = cL_\kappa/\kappa_0$ is the wave speed to diffusion speed ratio, and ϕ_0 drops out because (2) is linear.

[15] The initial location of the tracer center of mass is at $x = 0$ and L_0 is the length scale of the dimensional initial condition so that $\hat{\phi}(x/L_0, t = 0) = \hat{\phi}(\hat{x}/(L_0/L_\kappa), \hat{t} = 0)$. This gives an additional parameter L_0/L_κ , the ratio of initial condition to bore length scale. Thus the single bore tracer dispersion model has four dimensional parameters, (c , κ_0 , L_κ , and L_0) but only two nondimensional parameters (\hat{c} and L_0/L_κ).

2.2. Multiple Bores

[16] In the surf zone, tracer is repeatedly hit by breaking waves, each contributing to cross-shore tracer dispersion. To include this effect, the simple model is extended to include a periodic breaking-wave train with period T (the fifth dimensional parameter) so that

$$\kappa = \sum_n \kappa_n [x - c(t + nT)].$$

which nondimensionalized is

$$\hat{\kappa} = \sum_n \hat{\kappa}_n [\hat{x} - \hat{c}(\hat{t} + n\hat{T})].$$

The nondimensional period $\hat{T} = T/\tau = \kappa_0 T/L_\kappa^2$, the ratio of the wave period to the diffusion timescale, is the third nondimensional parameter. For simplicity, random waves which result in bores with variable κ_0 and T are not considered.

2.3. Variable Depth

[17] Cross-shore variable surf zone depth affects the concentration of a vertically well-mixed tracer. For example, even with $\kappa = 0$, ϕ transported to deeper water must

decrease to conserve ($h\phi$). Variable depth also affects the bore phase speed and the intensity of mixing (i.e., κ_0 and L_κ). The next extension of the simple model considers a planar beach where $h = h_0 - \beta x$ where h_0 is the depth at the tracer release location $x = 0$, and β is the beach slope. This model is intended to represent a self-similar surf zone with well developed bores where the ratio of wave height to depth is roughly constant.

[18] Nondimensionalizing (1) results in

$$\partial_t [\hat{h}\hat{\phi}] = \partial_{\hat{x}} [\hat{\kappa}\hat{h}\partial_{\hat{x}}\hat{\phi}].$$

where \hat{h} is the nondimensional depth,

$$\hat{h} = \frac{h}{h_0} = 1 - (\beta L_\kappa/h_0)\hat{x} = 1 - \hat{\beta}\hat{x}, \quad (6)$$

and $\hat{\beta} = \beta L_\kappa/h_0$ is the nondimensional beach slope, the fourth nondimensional parameter. Depth variation makes c , κ_0 and L_κ functions of the cross-shore position, which is discussed in the next subsection.

2.4. Choosing the Parameters

[19] The dimensional parameters (c , κ_0 , L_κ , L_0 , T , and β) have limits in their range and are not independent, which has implications for the nondimensional parameters. The shallow water phase speed is $c = \sqrt{gh}$, and for the variable depth model $c = c_0(1 - \beta x)^{1/2}$ where $c_0 = \sqrt{gh_0}$. The wave period T on typical ocean beaches varies between 5 and 15 s, and the beach slope β typically varies between 0.01 and 0.1 for very steep beaches. However, steep beaches have a very narrow self-similar surf zone. Because self-similar surf zone regions are of interest, the smaller end of the β range (0.01 – 0.03) is examined. As the initial spreading of an initially narrow tracer distribution is of most interest, generally $L_0 \leq L_\kappa$ is considered. Larger L_0 tracer initial conditions are implicitly solved for in multiple bore simulations as the tracer patch grows.

[20] The choice for κ_0 and L_κ is more uncertain. Simple scalings are used that are found to agree with a more complicated model (section 4). The bore width L_κ is assumed to be proportional to the bore height which in a self-similar surf zone is proportional to the water depth h . Thus the scaling of $L_\kappa = O(1)h$ is chosen. By mixing length arguments [e.g., *Tennekes and Lumley, 1972*] $\kappa \sim Ul$ where U and l are turbulent velocity and length scales, respectively. Using c to scale the turbulent velocity and L_κ the turbulent length scale then $\kappa_0 = O(1)cL_\kappa$ and $\kappa_0 \sim (gh^3)^{1/2}$. Using different reasoning, *Inman et al. [1971]* arrived at the same κ_0 scaling. With these choices, the parameters c , κ_0 , and L_κ are all dependent upon h , collapsing the parameter choice.

[21] The nondimensional parameters and their dependencies are estimated from the κ_0 and L_κ scaling choices, constraining the parameter range for examining simple model solutions. The nondimensional bore phase speed $\hat{c} = cL_\kappa/\kappa_0 = O(1)$, indicating that the \hat{c} parameter range to explore is narrow. The nondimensional wave period $\hat{T} = \kappa_0 T/L_\kappa^2 = O(1)(g/h)^{1/2}T$. Given that T is constant from linear wave theory, \hat{T} only varies due to depth. The nondimensional beach slope $\hat{\beta} = \beta L_\kappa/h_0 = O(1)\beta$. The dimensional

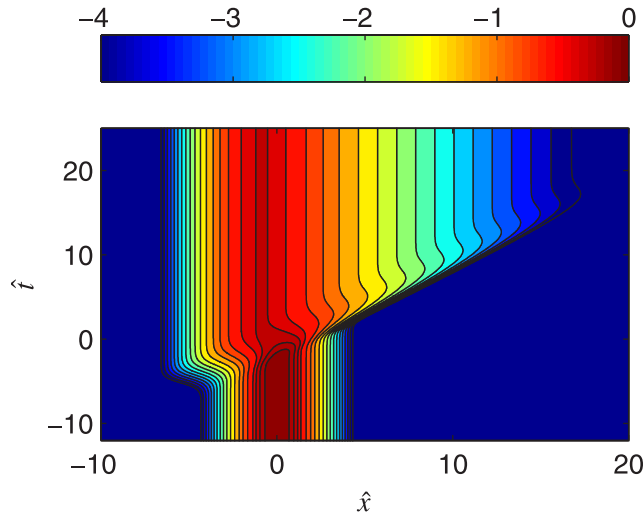


Figure 1. Log10 tracer $\hat{\phi}$ concentration as a function of \hat{x} and \hat{t} for the single bore simple model with $\hat{c} = 1$ and $L_0/L_\kappa = 1$. The concentration shading scheme spans 10^{-4} to 1.

and nondimensional scalings will be examined (section 4) from a Boussinesq surf zone wave model that includes wave breaking.

2.5. Tracer Moments

[22] To simplify the analysis, nondimensional moments of the cross-shore tracer distribution are used to describe the tracer evolution, in particular the tracer center of mass, width, skewness, and maximum concentration. The depth-integrated tracer moments are defined as

$$\langle f \hat{\phi} \rangle = \frac{\int f \hat{h} \hat{\phi} d\hat{x}}{\int \hat{h} \hat{\phi} d\hat{x}} \quad (7)$$

so that $\langle \hat{\phi} \rangle = 1$. For the single and multiple bores models, \hat{h} is constant and drops out of (7). The tracer center of mass is defined as $\bar{x}(\hat{t}) = \langle \hat{x} \hat{\phi} \rangle$, the tracer width $\sigma(\hat{t})$ as

$$\sigma(\hat{t}) = \left(\langle (\hat{x} - \bar{x})^2 \hat{\phi} \rangle \right)^{1/2},$$

and the skewness $S(\hat{t})$ as

$$S(\hat{t}) = \frac{\langle (\hat{x} - \bar{x})^3 \hat{\phi} \rangle}{\sigma^3}.$$

The “effective” cross-shore tracer diffusivity μ is

$$\mu = \frac{1}{2} \frac{d\sigma^2}{d\hat{t}}. \quad (8)$$

The maximum concentration, $\hat{\phi}_{\max} = \max(\hat{\phi})$, is an indication of tracer dilution. The dimensional tracer center of mass, width, and effective diffusivity are $L_\kappa \bar{x}$, $L_\kappa \sigma$, and $\kappa_0 \mu$, respectively.

3. Results

3.1. Single Bore

[23] The dispersion of a single bore propagating through a tracer patch is examined by solving the nondimensional

equation (4) over \hat{c} and L_0/L_κ parameter space with cross-shore model domain of $L_x = \pm 50$. The $\hat{\phi}$ solution with $\hat{c} = 1$ and $L_0/L_\kappa = 1$ is shown in Figure 1. At $\hat{t} = 0$, the propagating bore arrives at the center of the tracer patch ($\hat{x} = 0$). As it reaches the offshore side of the tracer, the bore diffuses tracer farther offshore ($-3 < \hat{t} < 0$). This process halts as the bore moves shoreward and continually disperses and dilutes the onshore edge of tracer further onshore ($0 < \hat{t} < 15$). With the bore passed, the resulting $\hat{\phi}$ is spread out significantly and diluted ($\hat{\phi}_{\max}$ is reduced by 50%). The resulting $\hat{\phi}$ is no longer symmetric, with weak tracer concentrations spread shoreward to $\hat{x} = 15$. The $\hat{\phi}$ solutions for other values of \hat{c} and L_0/L_κ are qualitatively similar to those for $\hat{c} = 1$ and $L_0/L_\kappa = 1$ (Figure 1). Only the amount of cross-shore dispersion, dilution, and skewness change.

[24] The effect of varying \hat{c} and L_0/L_κ are examined through the tracer moments \bar{x} , σ , S , and $\hat{\phi}_{\max}$ (Figures 2 and 3). For all \hat{c} and L_0/L_κ choices, the net effect of a single bore on \bar{x} is minimal (Figure 2a and Figure 3a). Dimensionally, the tracer center of mass is not displaced more than a bore half-width L_κ . When the bore arrives at the tracer, \bar{x} temporarily is slightly negative. In this model a bore does not advect (or “surf”) tracer onshore. The σ increase is larger for smaller \hat{c} (Figure 2b), reflecting the longer time the bore has for diffusion. The relative (to $\hat{t} = 0$) σ increase

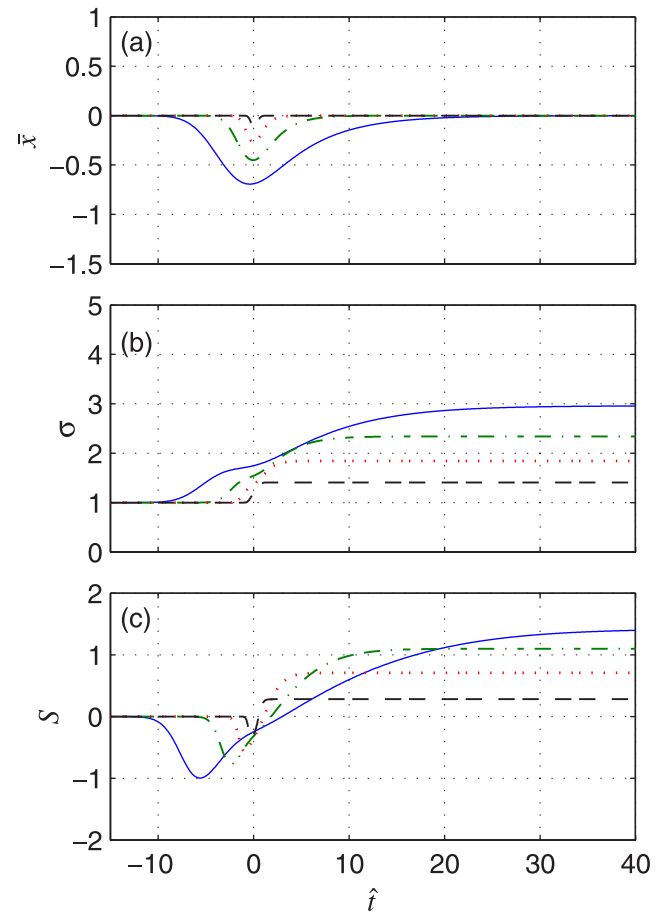


Figure 2. (a) Mean tracer position \bar{x} , (b) standard deviation σ , and (c) skewness S versus \hat{t} for the single bore simulations with $L_0/L_\kappa = 1$ and $\hat{c} = [0.5, 1, 2, 5]$ (solid, dash-dotted, dotted, and dashed, respectively).

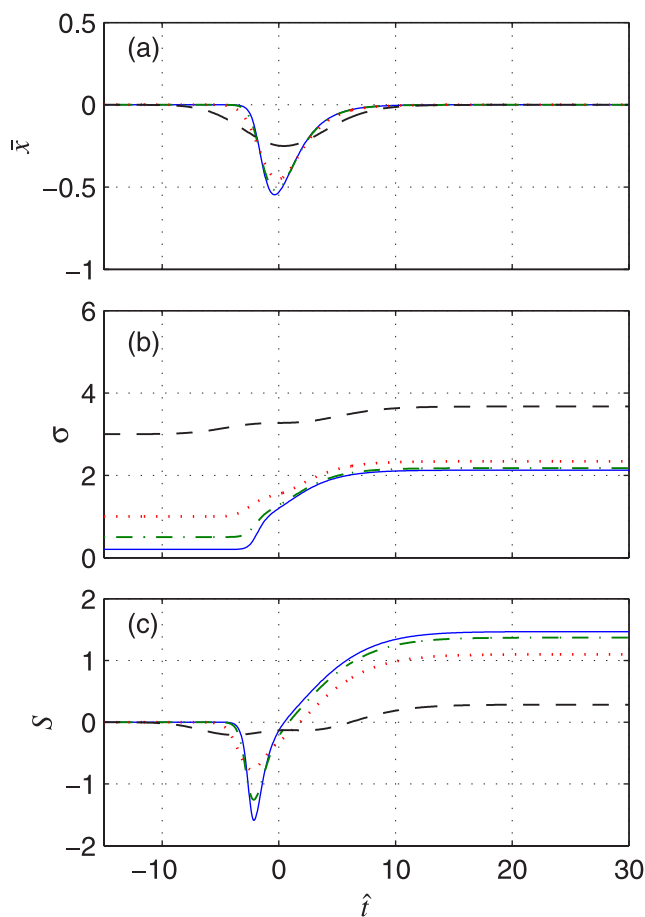


Figure 3. The (a) \bar{x} , (b) σ , and (c) S versus \hat{t} for the single bore simulations with $\hat{c} = 1$ and $L_0/L_\kappa = [0.2, 0.5, 1, 3]$ (solid, dash-dotted, dotted, and dashed, respectively).

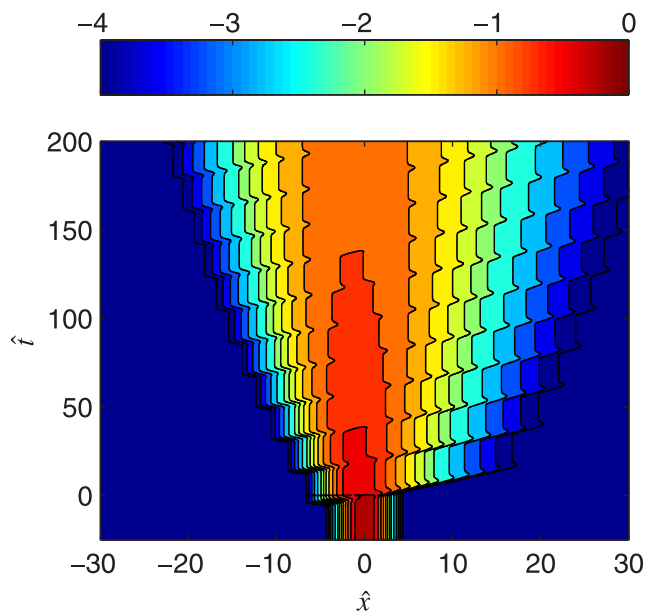


Figure 4. Log10 tracer $\hat{\phi}$ concentration as a function of nondimensional \hat{x} and \hat{t} for the flat bottom, multiple bore simulations with $\hat{c} = 1$ and $\hat{T} = 20$. The concentration shading scheme spans 10^{-4} to 1.

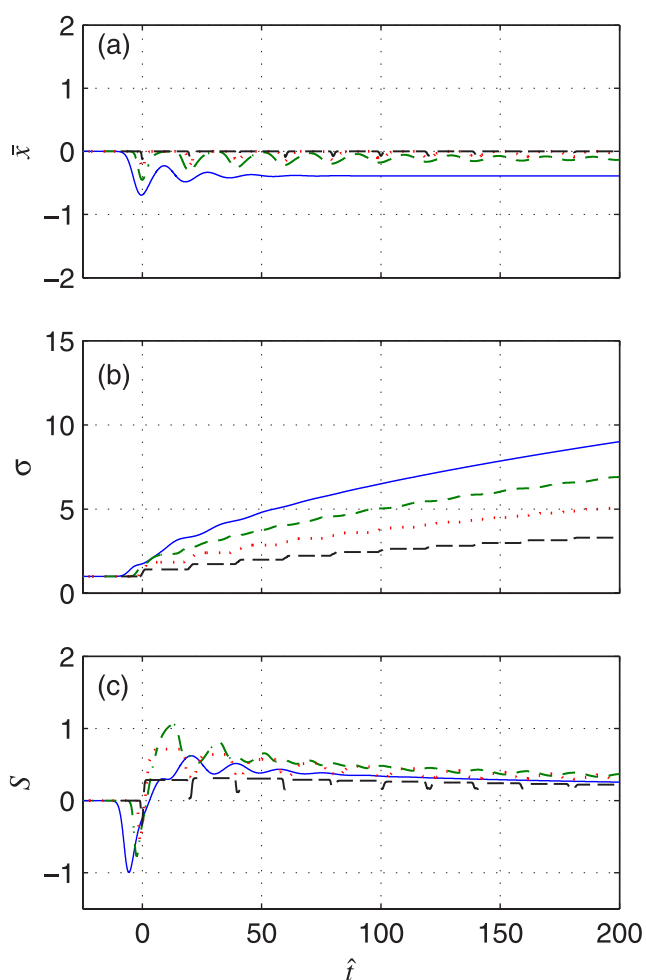


Figure 5. The (a) \bar{x} , (b) σ , and (c) S versus \hat{t} for multiple bore simulations with $\hat{c} = [0.5, 1, 2, 5]$ (solid, dash-dotted, dotted, and dashed, respectively), $L_0/L_\kappa = 1$, and $\hat{T} = 20$.

is greater for smaller L_0/L_κ (Figure 3b). The tracer dilution, indicated by the $\hat{\phi}_{\max}$ reduction is also larger for smaller \hat{c} and L_0/L_κ (not shown). For all cases $\hat{\phi}_{\max} \sim \sigma^{-1}$ as would be expected for a cross-shore Gaussian tracer profile. With the bore arrival ($\hat{t} \leq 0$), the skewness initially becomes negative, but with the passage the bore ($\hat{t} > 0$), significant positive skewness is induced (Figures 2c and 3c) as weakly concentrated tracer is spread onshore (e.g., Figure 1). The final S is larger with smaller and smaller L_0/L_κ . When $L_0/L_\kappa \gg 1$, a single bore does not significantly increase σ or create skewness.

3.2. Multiple Bores

[25] The effect of multiple bores with the simple model is examined next. There are three nondimensional parameters (\hat{c} , \hat{T} , L_0/L_κ) to vary. To reduce parameter space $L_0/L_\kappa = 1$ is kept fixed. Tracer $\hat{\phi}$ solution with $\hat{c} = 1$ and $\hat{T} = 20$ is shown in Figure 4. The tracer spreading due to each bore is evident in the sharp diagonal ridges. The tracer center of mass remains near zero, cross-shore dispersion has become quasi-continuous, and (after 2–3 waves) largely symmetric.

[26] The tracer moments \bar{x} , σ , and S are examined for variable \hat{c} and constant \hat{T} (Figure 5) and for constant \hat{c} and variable \hat{T} (Figure 6). For all \hat{c} and \hat{T} , \bar{x} remains near zero

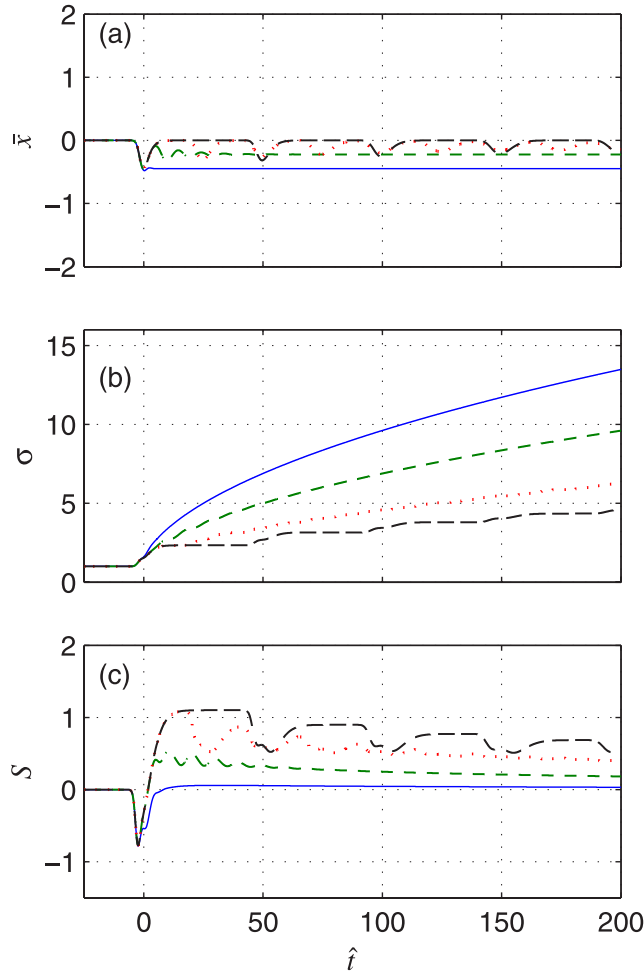


Figure 6. The (a) \bar{x} , (b) σ , and (c) S versus \hat{t} for multiple bore simulations with $\hat{c} = 1$, $L_0/L_\kappa = 1$, and $\hat{T} = [5, 10, 25, 50]$ (solid, dash-dotted, dotted, and dashed, respectively).

(Figure 5a and Figure 6a). Dimensionally, the tracer center of mass moves less than a bore half-width L_κ . Similar to the single bore model, σ grows faster for smaller \hat{c} (Figure 5b) and for smaller \hat{T} (Figure 6b) as more bores disperse the tracer in a period of time. With multiple bores, the quasi-continuous dispersion scales as $\sigma^2 \sim \alpha(\hat{c}, \hat{T})\hat{t}$ where the slope α depends upon \hat{c} and \hat{T} and the linear time dependence is that expected for a constant (in x and t) κ . As the first bores hit the tracer near $\hat{t} = 0$, S initially becomes negative and then positive (Figure 5c and 6c). However, as seen in the $\hat{\phi}$ solution (Figure 4), after multiple bores pass, S approaches zero. This happens more rapidly with smaller \hat{T} and \hat{c} .

3.3. Multiple Bores and Planar Beach

[27] The effect of periodic bores and a planar beach is examined next and the beach slope is now an additional parameter. In general the dimensional and nondimensional parameters vary in the cross-shore, the tracer dispersion will be described using the parameters (e.g., \hat{c} and \hat{T}) at $x = 0$. Solutions are found over a wide range of \hat{c} (0.5–4), \hat{T} (8–60), and $\hat{\beta}$ (0–0.0037) with fixed $L_0/L_\kappa = 1$ for a total of 216 model runs. The onshore end of the model domain varies depending on the parameter choices. Model solutions

are examined up until the time that shoreline ϕ reaches 2% of $\hat{\phi}_{\max}$. Before this time, the boundary is not expected to significantly influence tracer evolution. For most of the model runs, the shoreline ϕ is $<0.001\hat{\phi}_{\max}$ at $\hat{t} = 200$.

[28] Tracer solutions with a planar beach are similar to those with a flat bottom (e.g., Figure 4). The mean and standard deviation of the tracer statistics \bar{x} , σ , and S from all 216 model runs are shown in Figure 7. Over all parameter range, the tracer moments mirror those of the flat bottom periodic bore simulations (Figures 5 and 6). This includes that \bar{x} remains near zero (Figure 7a), $\sigma \sim t^{1/2}$ (Figure 7b), and with nonzero skewness with the first bore's passage, but then skewness evolves toward zero (Figure 7c). The reduction in $\hat{\phi}_{\max}$ is consistent with the growth in σ (i.e., $\hat{\phi}_{\max} \sim \sigma^{-1}$, not shown).

[29] In general, the tracer length scale squared grows like $\sigma^2 \sim \alpha(\hat{c}, \hat{T}, \hat{\beta})\hat{t}$. The value of α is inferred by fitting a constant slope to the observed linear $\sigma^2 - \hat{t}$ dependence. The skill of fit is high (>0.9) in all cases. The best-fit slope $\alpha(\hat{c}, \hat{T}, \hat{\beta} = 0)$ and $\alpha(\hat{c}, \hat{T}, \hat{\beta} = 0.037)$ are shown in Figure 8. The dependence of α upon $\hat{\beta}$ is weak (compare Figures 8a and 8b). Thus bore-induced dispersion rate does not depend significantly on nondimensional beach slope. Over this \hat{c}

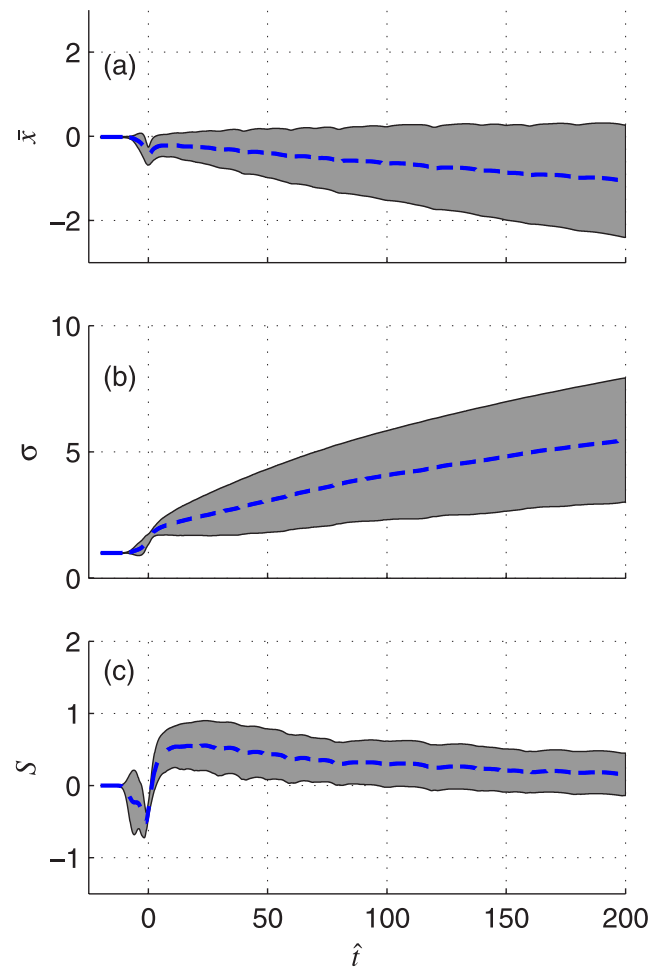


Figure 7. The (a) \bar{x} , (b) σ , and (c) S versus \hat{t} for multiple bore and planar beach simulations with $\hat{c} = [0.5, 1, 2, 4]$, $\hat{T} = [20, 40, 60, 80]$, $\hat{\beta} = [0, 0.0123, 0.0245, 0.0368]$ and $L_0/L_\kappa = 1$.

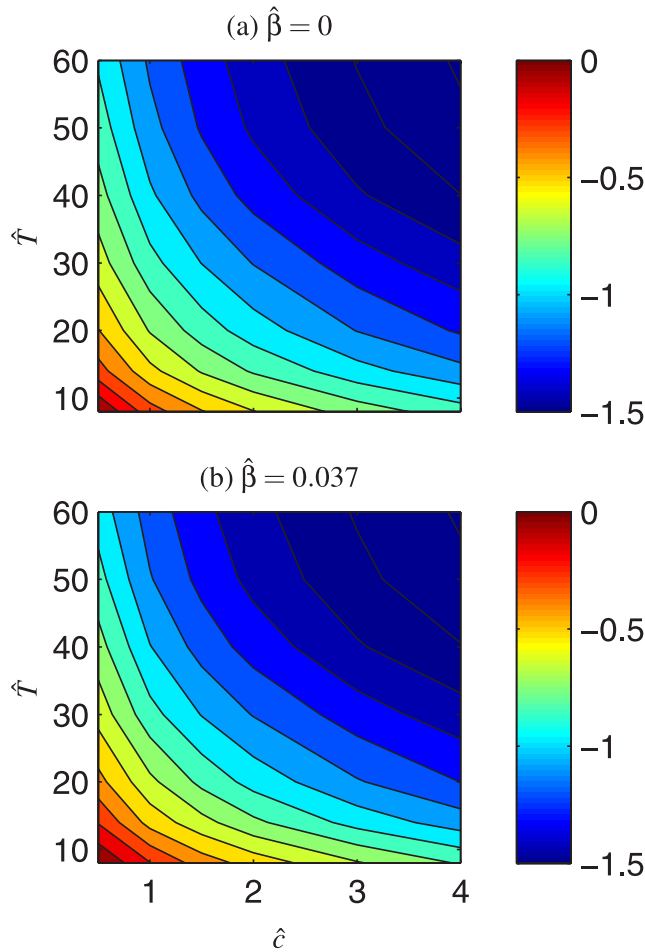


Figure 8. Contour plot of $\log_{10}(\alpha)$ as a function of \hat{c} and \hat{T} for (a) $\hat{\beta} = 0$ and (b) $\hat{\beta} = 0.037$.

and \hat{T} parameter range, α varies between 0.03 and 1, resulting in nondimensional bulk diffusivities μ of 0.015–0.5. As mentioned in section 3.2, α is larger for smaller \hat{c} and smaller \hat{T} , and the form of α can be represented functionally as $\alpha \sim (\hat{c}\hat{T})^{-1}$.

4. Boussinesq Model Results

[30] The simple model for breaking-wave induced cross-shore tracer dispersion is rather simplified. For example, orbital wave motions, that have potential to increase bore-induced dispersion via tracer stretching, are not included. The form for the bore diffusivity (3) and the assumed scalings for $\kappa_0 \sim (gh^3)^{1/2}$ and $L_\kappa \sim h$ are also simplifications. A surf zone Boussinesq wave model is coupled with a tracer evolution equation to further study breaking-wave induced tracer dispersion and to validate (relative to the more complex Boussinesq model) the simple model results.

[31] The Boussinesq model used is similar to the FUNWAVE [e.g., *Chen et al.*, 1999] model. The extended Boussinesq equations of *Nwogu* [1993] (with nonlinearity and higher order dispersion valid in intermediate water depths) are implemented with a breaking-wave eddy viscosity scheme [*Zelt*, 1991; *Kennedy et al.*, 2000]. Essentially, when the front face of the wave is sufficiently

steep, the eddy viscosity becomes nonzero and wave energy is reduced. Similar Boussinesq models have been used successfully to simulate laboratory rip currents [*Chen et al.*, 1999], the cross-surf zone structure of laboratory monochromatic and random waves [*Kennedy et al.*, 2000; *Lynett*, 2006], and alongshore currents in the field [*Chen et al.*, 2003]. As with the simple model, the Boussinesq model assumes alongshore uniform conditions.

[32] Coupled to the Boussinesq model is a depth-averaged tracer conservation equation, similar to (4), which includes the full instantaneous water depth $h + \eta$ (η is the free-surface elevation) and the advection due to orbital wave motions, i.e.,

$$\partial_t[(h + \eta)\phi] + \partial_x[(h + \eta)u\phi] = \partial_x[\kappa_{br}(h + \eta)\partial_x\phi] \quad (9)$$

where u is the cross-shore velocity of the Boussinesq model (at a fixed relative-depth) and with small kh is very close to the depth-averaged velocity. The bore induced eddy diffusivity κ_{br} is set equal to the breaking-wave eddy viscosity which assumes that momentum and tracer are mixed identically; the tracer Schmidt number is one. Similar to the simple model, (9) assumes a vertically uniform tracer and bore-induced mixing throughout the water column.

[33] The surf zone Boussinesq model cross-shore domain is 600 m and the grid size $\Delta x = 0.5$ m. The model is run on two different beach slopes: a shallow slope (denoted as case one) with $\beta_1 = 0.015$ and a steeper slope (case two) of $\beta_2 = 0.025$. Upon reaching 6 m water depth (385 m and 230 m from shore respectively), the bathymetry is flat out to the offshore boundary. Sponge layers on both onshore and offshore boundaries absorb wave energy preventing wave reflection. Monochromatic waves of height $H = 1$ m and different wave periods (for β_1 : $T = 6, 8, 10, 12.5, 15$ s; for β_2 : $T = 6, 8, 10, 12.5$ s) representative of natural surf zones are generated 550 m from the shoreline in $h = 6$ m depth following *Wei et al.* [1999]. Simulations with $T = 15$ s on slope β_2 are not included in the analysis because a self-similar surf zone was not produced by the Boussinesq model.

[34] Example Boussinesq model output is shown in Figure 9. Waves with $T = 8$ s approach shore, shoal (not shown), and break (Figure 9a) on the planar bathymetry (Figure 9d). The breaking-wave induced eddy diffusivity κ_{br} , associated with the front face of the breaking waves, decreases in magnitude in shallower water (Figure 9b). After the model reaches quasi-steady conditions, a delta function of tracer ϕ is released 75 m from shore (dashed curve in Figure 9c). After 200 s, the tracer has spread (solid curve in Figure 9c) in a largely symmetric fashion.

[35] Both the shallow (case one) and steep (case two) beach slope runs have a self-similar surf zone region where $\gamma = H/h$ is constant (Figure 10). The wave height is defined as $H = 2\sqrt{2}\sigma_\eta$, where σ_η^2 is the sea-surface elevation variance. For both beach slopes, the best fit $\gamma = 0.52$. The self-similar regions are 40–120 m (case one) and 20–75 m (case two) from the shoreline. The subsequent dispersion analysis is restricted to these regions.

[36] To examine the presumed scalings of the dimensional simple model parameters, κ_0 and L_κ are inferred from the Boussinesq model runs as a function of cross-shore position. In any model run, each bore (i.e., a local maxima of eddy diffusivity) within the self-similar surf zone region

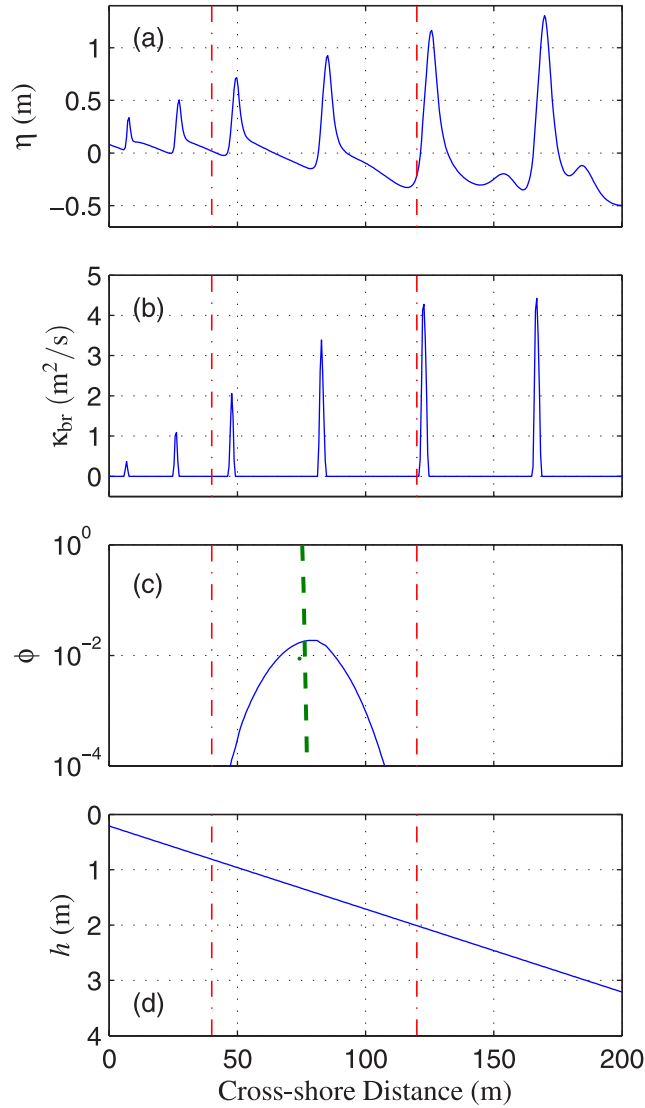


Figure 9. (a) Free-surface elevation η , (b) breaking wave eddy diffusivity κ_{br} , (c) tracer ϕ , and (d) depth h versus cross-shore distance for the model at $t = 200$ s after the tracer is released. The dashed curve in Figure 9c is the tracer concentration 1 s after release at 75 m from shore. The incoming $H = 1$ m and $T = 8$ s. The beach is planar with slope $\beta = 0.015$ (case one). The horizontal dash-dotted lines bound the self-similar surf zone region.

had it's the maximum κ (κ_0) and length scale (L_{κ} , $1/2$ of the e -folding distance) recorded at the bore's cross-shore location. As the bore propagates onshore, its κ_0 and L_{κ} are continuously recorded at the location of κ_0 . At each cross-shore location, these values were averaged together to yield representative κ_0 and L_{κ} estimates. The scalings of $\kappa_0 \sim (gh^3)^{1/2}$ (Figure 11a) and $L_{\kappa} \sim h$ (Figure 11b) are largely followed, consistent with the assumptions in section 2.4. Both κ_0 and L_{κ} are larger for increased dimensional wave period T . The resulting mixing timescale $\tau = L_{\kappa}^2/\kappa_0$ varies between 0.25 and 0.5 s.

[37] With the L_{κ} and κ_0 estimates and $c = (gh)^{1/2}$, the three nondimensional parameters (\hat{c} , \hat{T} , and $\hat{\beta}$) are estimated within the self-similar surf zone region (Figure 12). For both

beach slopes, the inferred is near one (as hypothesized) and increases slightly in shallower water (Figures 12a and 12b). For β_1 (β_2), \hat{c} varies between 1 and 2 (1–1.5). The κ_0 and L_{κ} variation with T (Figure 11), results in larger for smaller wave periods. For both beach slopes, the nondimensional wave period \hat{T} varies between 10–40 decreasing slightly in shallower water (Figures 12c and 12d). The nondimensional beach slope $\hat{\beta}$ varies between 0.01 and 0.04 (about $\pm 50\%$ of β) increasing in shallower water (Figures 12e and 12f).

[38] After the model reaches quasi-steady conditions, initial delta functions of tracer were released at various cross-shore locations to sample a variety of c , κ_0 , and L_{κ} (e.g., Figure 11). For slope β_1 , there were three release locations (50, 75, and 100 m from the shoreline) in the self-similar surf zone region. The steeper slope β_2 has four tracer releases (30, 40, 50, 60 m from the shoreline) for the $T = 6, 8$ s periods and three tracer releases (at 30, 40, 50 m from the shoreline) for the $T = 10, 12.5$ s periods. Release locations were chosen so that tracer remained within the self-similar surf zone region for analysis. Nondimensional moment statistics (\bar{x} , σ , and S) for each run are calculated using the dimensional parameters (L_{κ} and κ_0) at the release location and replacing h with $h + \eta$ in (7). With a delta function release $L_0/L_{\kappa} \rightarrow 0$.

[39] The evolution of the Boussinesq model moments mirror those of the simple model (section 3). The Boussinesq model \bar{x} does not vary much from zero (Figures 13a and 13b), although \bar{x} becomes on average slightly positive and oscillates due to the advective effects of surface gravity waves. Similar to the simple model, on average the Boussinesq model tracer width $\sigma \sim \hat{t}^{1/2}$, with oscillations due to wave orbital motions (Figures 13c and 13d). The σ growth rate does not vary substantially between the two beach slopes (note the different abscissas on left and right columns of Figure 13) and is consistent with the earlier simple model results (e.g., Figure 7). Tracer dilution is consistent with the σ increase (i.e., $\phi_{max} \sim \sigma^{-1}$). In all cases, skewness becomes nonzero with the passage of the

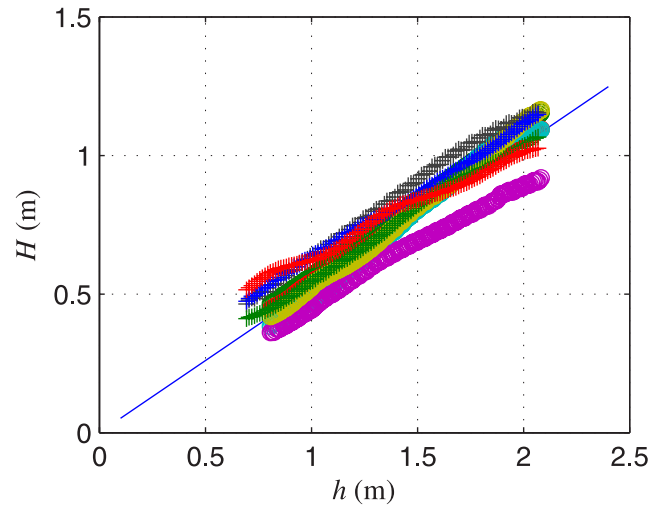


Figure 10. Wave height H versus water depth h for the β_1 and β_2 beach slope runs. The best-fit line with slope of $\gamma = 0.52$ is shown, and the shading represent model runs with different β and T .

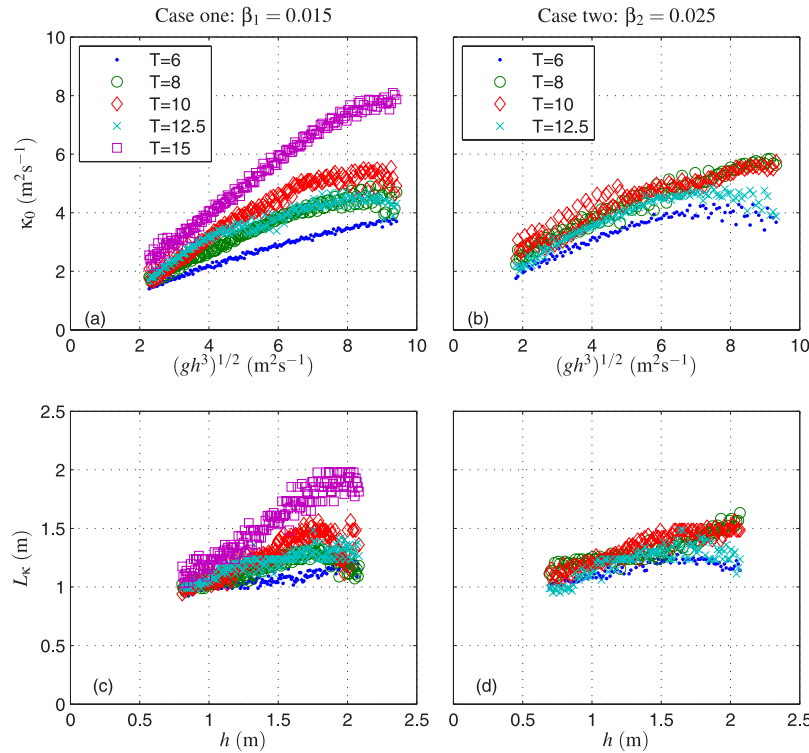


Figure 11. (a,b) Boussinesq model inferred κ_0 versus $(gh^3)^{1/2}$ and (c,d) L_{κ} versus h for case one $\beta_1 = 0.015$ (left column) and case two $\beta_2 = 0.025$ (right column). Only the region of the self-similar surf zone is shown.

first bore. The large magnitudes of S are due to $L_0/L_{\kappa} \rightarrow 0$. For a single bore S depends strongly on L_0/L_{κ} (Figure 3c). However, after the second bore passes, S slowly goes to zero as with the simple model results (Figure 7c).

[40] The simple model is run with nondimensional parameters that are approximate cross-shore means of \bar{x} , σ , and S (Figure 12). For case one, $\hat{c} = 1.5$, $\hat{T} = 30$, $\hat{\beta} = 0.015$, and for case two, $\hat{c} = 1.25$, $\hat{T} = 25$, $\hat{\beta} = 0.025$. For both, $L_0/L_{\kappa} = 0.1$. With these parameters, the simple (thick dashed lines in Figure 13) and Boussinesq model results compare favorably. The reduced dynamics of the simple model largely capture the statistics of bore-induced dye dispersion and suggests that the assumptions used in the simple model (relative to the Boussinesq model) are reasonable.

[41] The lack of scatter in the Boussinesq model σ is surprising given the \hat{c} and \hat{T} variation (Figures 12a–12d) and the simple model results showing the strong α dependence on both (Figure 8). For example, for both cases at $\hat{t} = 150$, σ mostly varies between 4 and 6, whereas the simple model results indicated larger variation (Figure 6). To explore this further, the Boussinesq model \hat{c} is plotted versus \hat{T} (Figures 12a–12d) superimposed upon $\log_{10}[\alpha(\hat{c}, \hat{T})]$ contours in Figure 14. For both beach slopes, an inverse relationship exists between \hat{c} and \hat{T} . This results in a smaller α range than with fixed \hat{c} and the same \hat{T} variation, and explains the similarity of the Boussinesq model σ . The inverse variation of \hat{c} and \hat{T} is due in part to L_{κ}/κ_0 appearing in the numerator and denominator of \hat{c} and \hat{T} , respectively. Thus these two nondimensional parameters are not independent.

[42] The small α variation due to the inverse \hat{c} - \hat{T} relationship suggests that within a self-similar surf zone non-dimensional tracer dispersion (and the bulk nondimensional diffusivity μ) is approximately independent of cross-shore position. In the self-similar region, dimensional tracer dispersion, with bulk diffusivity $\kappa_0\mu$, is faster farther offshore.

5. Discussion

[43] The principal results, near-constant \bar{x} , $\sigma^2 \sim \alpha(\hat{c}, \hat{T})\hat{t}$, and characterizing the skewness evolution, provide practical testable hypotheses for laboratory or field observations of breaking-wave induced tracer dispersion. Some of these features were observed in limited laboratory surf zone observations of cross-shore tracer dispersion [Pearson *et al.*, 1997]. Dye tracer was injected into the surf zone with normally incident waves and a forced (pumped) steady alongshore current. Cross-shore tracer transects were measured downstream (alongshore) of the injection location so that alongshore distance becomes a proxy for time. As it was advected downstream, the mean cross-shore tracer position (\bar{x}) was constant within measurement precision. Tracer spread in both onshore and offshore directions, but the information given is insufficient to infer whether the $\sigma^2 \sim \hat{t}$ scaling applies. At the first transect downstream from the injection point (i.e., short time), the tracer profile is skewed, but farther downstream (i.e., long time) it becomes more symmetric. Although limited, the Pearson *et al.* [1997] laboratory study provides preliminary support for this bore-induced tracer dispersion model.

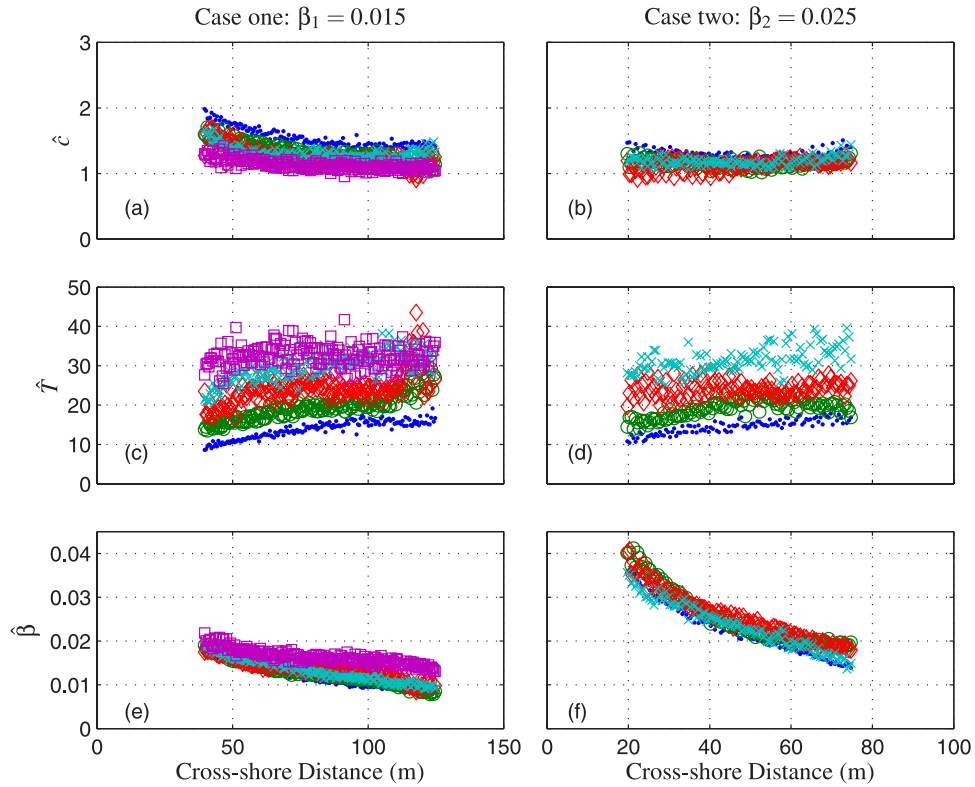


Figure 12. Boussinesq model inferred (a,b) \hat{c} , (c,d) \hat{T} , and (e,f) $\hat{\beta}$ versus x for case one $\beta_1 = 0.015$ (left column) and case two $\beta_2 = 0.025$ (right column). The symbols are the same as for Figure 11. Only the region of the self-similar surf zone is shown.

[44] Both simple and Boussinesq models use an eddy diffusivity associated with the breaking wave. It is not known whether this mechanism for tracer dispersion is realistic. However, the cross-shore structure of free-surface elevation for both monochromatic and random laboratory breaking waves is accurately modeled with this breaking mechanism [Kennedy *et al.*, 2000; Lynett, 2006]. Thus it stands to reason a bore associated tracer eddy diffusivity also is applicable with an $O(1)$ Schmidt number, here chosen to be one.

[45] An alternative breaking-wave tracer dispersal paradigm is the wave roller [e.g., Fredsoe and Deigaard, 1992]. Qualitatively tracer would be entrained into the roller, stored, advected shoreward, and leaked out as the bore propagates onshore. Below the trough level, offshore directed undertow (balancing the onshore roller mass flux) would transport residual tracer offshore. The next roller would repeat this process, conceptually resulting in depth-integrated tracer dispersion. Wave roller models are invoked to move wave forcing maxima shoreward which improve agreement of models to alongshore current observations [e.g., Reniers and Battjes, 1997; Ruessink *et al.*, 2001; Feddersen *et al.*, 2004]. Wave roller models also have been successfully used to model wave breaking in a Boussinesq model [e.g., Schäffer *et al.*, 1993].

[46] There are other limitations and assumptions to the simple model. For example, it only applies in a self-similar surf zone region. Tracer dispersion outside this region is not considered. In isolating only breaking-wave induced tracer dispersion, all other surf zone dispersion mechanisms (e.g.,

shear waves, wave group forced circulation, surf zone vortices) are neglected. Bore-induced cross-shore dispersion likely has a dominant effect on timescales of a few wave periods but shorter than the longer timescales (100's of seconds) which contribute most to surf zone drifter dispersion [Spydell *et al.*, 2007]. Recall that drifters do not feel the dispersive effects of the bore.

[47] Perhaps the most questionable assumption is that of depth-uniform tracer and eddy diffusivity. The vertical distribution of tracer in the surf zone has not been quantitatively measured, and thus there is no way of knowing the quality of this assumption. Qualitative surf zone dye observations by the author and colleagues suggest that after a bore or two, dye released at the surface is fairly well mixed in the vertical. In addition, the bore's diffusivity is clearly not vertically uniform and is related to the turbulence under surf zone breaking waves. In both laboratory [e.g., Ting and Kirby, 1994] and field [George *et al.*, 1994; Bryan *et al.*, 2003] surf zone observations, turbulence (inferred through a variety of techniques) is stronger near the surface. However, turbulence is elevated over the entire water column. The potential error in assuming depth-uniformity is qualitatively diagnosed by splitting both κ and ϕ into depth-average (i.e., $\bar{\kappa}$ and $\bar{\phi}$) and vertical fluctuations (i.e., κ' and ϕ'), resulting in a bore-induced diffusion term (replacing the right-hand side of equation (1))

$$\partial_x [\bar{\kappa}(h + \eta)\partial_x \bar{\phi}] + \partial_x \left[\int_{-h}^{\eta} \kappa' \partial_x \phi' dz \right]. \quad (10)$$

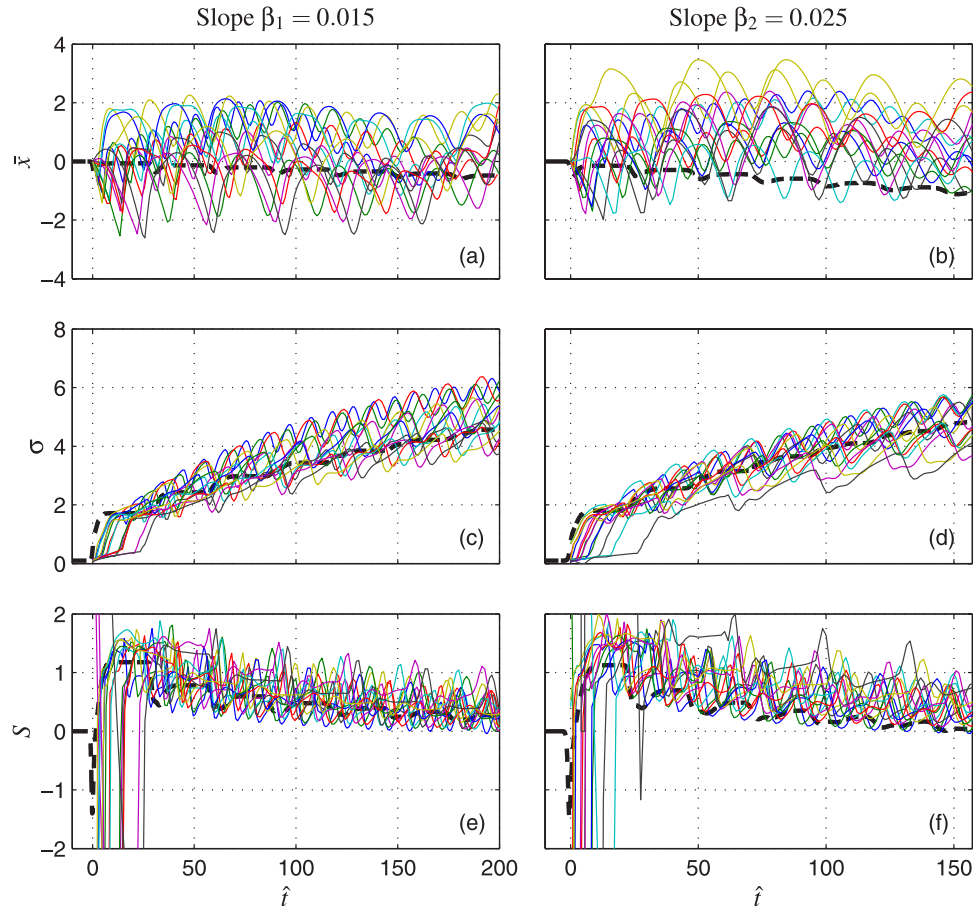


Figure 13. Boussinesq model tracer statistics with $\beta = 0.015$ (left column) and $\beta = 0.025$ (right column) (a,b) \bar{x} , (c,d) σ , and (e,f) S versus nondimensional time \hat{t} . The thick dashed curve is the simple model with $\hat{c} = 1.5$, $\hat{T} = 30$, and $\hat{\beta} = 0.015$ (left column) and $\hat{c} = 1.25$, $\hat{T} = 25$, and $\hat{\beta} = 0.0035$ (right column). The other curves are the various Boussinesq model solutions.

where z is the vertical coordinate. Thus the error in assuming depth uniformity is in part due to the vertical covariation of diffusivity and tracer gradients. Although certainly nonzero, there is no way to account for this yet.

6. Summary

[48] A simple model for breaking-wave induced cross-shore tracer dispersion is developed based upon the diffusion equation with a eddy diffusivity that propagates with bores. The model assumes depth uniform tracer and bore-induced mixing. Three levels of the model were developed: (1) single bore, (2) multiple bores, and (3) multiple bores with planar bathymetry. The dimensional and nondimensional parameters that govern the problem were identified, and scalings were developed.

[49] Solutions to the single bore model help to characterize the solutions to the more complicated multiple bore models. With multiple bores (in both flat and sloping bottoms) the principal results are (1) The tracer center of mass stays nearly constant. (2) The nondimensional tracer width (length-scale) squared scales as $\sigma^2 \sim \alpha(\hat{c}, \hat{T})\hat{t}$ where the slope α depends on nondimensional phase speed and wave period \hat{T} . (3) The skewness initially becomes nonzero

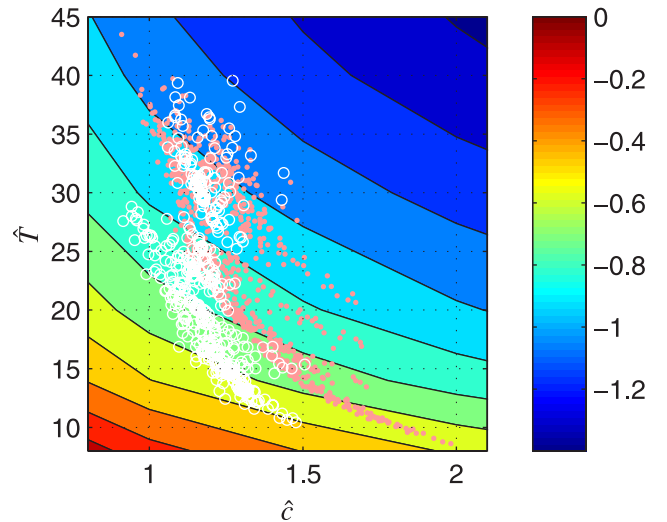


Figure 14. Boussinesq model inferred \hat{T} versus \hat{c} for slope β_1 (dots) and β_2 (circles) contoured upon $\log_{10}[\alpha(\hat{c}, \hat{T})]$ for $\hat{\beta} = 0.0245$.

with the passage of the first bore but returns to zero with the passage of subsequent bores.

[50] Tracer dispersion is also modeled with a much more sophisticated Boussinesq wave model that includes wave breaking for a range of beach slopes, wave periods, and tracer release locations. The scalings (developed earlier) for the dimensional parameters governing the dispersion are verified and the nondimensional parameters range is found. The tracer dispersion moments from the Boussinesq model solutions and the simple model agree well. The various Boussinesq model solutions have nondimensionally similar tracer dispersion growth rates. This is a result of an inverse relationship between \hat{c} and \hat{T} , and suggests that in general nondimensional tracer dispersion is uniform across a self-similar surf zone region. Although the model has limitations, these results provide testable hypotheses regarding breaking-wave driven cross-shore tracer dispersion for future investigation.

[51] **Acknowledgments.** This research was supported by the Office of Naval Research and CA Sea Grant. Matthew Spydell provided inspiration and code. R. T. Guza, Stephen Henderson, Marissa Yates, Dave Clark, and an anonymous reviewer all provided valuable feedback.

References

- Allen, J. S., P. A. Newberger, and R. A. Holman (1996), Nonlinear shear instabilities of alongshore currents on plane beaches, *J. Fluid Mech.*, *310*, 181–213.
- Boehm, A. B., S. B. Grant, J. H. Kim, C. D. McGee, S. Mowbray, C. Clark, D. Foley, and D. Wellmann (2002), Decadal and shorter period variability of surfzone water quality at Huntington Beach, California, *Environ. Sci. Technol.*, *36*, 3885–3892.
- Bowen, A. J., and R. A. Holman (1989), Shear instabilities of the mean longshore current: 1. Theory, *J. Geophys. Res.*, *94*, 18,023–18,030.
- Bowen, A. J., and D. L. Inman (1974), Nearshore mixing due to waves and wave-induced currents, *Rapp. P.-v Reun. Cons. Int. Explor. Mer*, *167*, 6–12.
- Bryan, K. R., K. P. Black, and R. M. Gorman (2003), Spectral estimates of dissipation rate within and near the surf zone, *J. Phys. Oceanogr.*, *33*, 979–993.
- Chen, Q., R. A. Dalrymple, J. T. Kirby, A. B. Kennedy, and M. C. Haller (1999), Boussinesq modeling of a rip current system, *J. Geophys. Res.*, *104*, 20,617–20,637.
- Chen, Q., J. T. Kirby, R. A. Dalrymple, F. Shi, and E. B. Thornton (2003), Boussinesq modeling of longshore currents, *J. Geophys. Res.*, *108*(C11), 3362, doi:10.1029/2002JC001308.
- Feddersen, F., R. T. Guza, and S. Elgar (2004), Inverse modeling of one-dimensional setup and alongshore current in the nearshore, *J. Phys. Oceanogr.*, *34*, 920–933.
- Fredsoe, J. and R. Deigaard (1992), *Mechanics of Coastal Sediment Transport*, World Sci., River Edge, N. J.
- George, R., R. E. Flick, and R. T. Guza (1994), Observations of turbulence in the surf zone, *J. Geophys. Res.*, *99*, 801–810.
- Grant, S., J. H. Kim, B. H. Jones, S. A. Jenkins, J. Wasyl, and C. Cudaback (2005), Surf zone entrainment, along-shore transport, and human health implications of pollution from tidal outlets, *J. Geophys. Res.*, *110*, C10025, doi:10.1029/2004JC002401.
- Haile, R. W., et al. (1999), The health effects of swimming in ocean water contaminated by storm drain runoff, *Epidemiology*, *10*, 355–363.
- Herterich, K., and K. Hasselmann (1982), The horizontal diffusion of tracers by surface waves, *J. Phys. Oceanogr.*, *12*, 704–711.
- Inman, D. L., R. J. Tait, and C. E. Nordstrom (1971), Mixing in the surf zone, *J. Geophys. Res.*, *26*, 3493–3514.
- Jiang, S. C., and W. Chu (2004), PCR detection of pathogenic viruses in Southern California urban rivers, *J. Appl. Microbiol.*, *97*, 17–28.
- Johnson, D., and C. Pattiaratchi (2004), Application, modelling and validation of surfzone drifters, *Coastal Eng.*, *51*, 455–471.
- Johnson, D., and C. Pattiaratchi (2006), Boussinesq modelling of transient rip currents, *Coastal Eng.*, *53*, 419–439.
- Kennedy, A. B., Q. Chen, J. T. Kirby, and R. A. Dalrymple (2000), Boussinesq modeling of wave transformation, breaking and runup. I: One dimension, *J. Waterway Port Coastal Ocean Eng.*, *126*, 39–47.
- Lynett, P. (2006), Nearshore modeling using high-order Boussinesq equations, *J. Waterway Port Coastal Ocean Eng.*, *132*, 348–357.
- Monismith, S. G., and D. A. Fong (2004), A note on the potential transport of scalars and organisms by surface waves, *Limnol. Oceanogr.*, *49*, 1214–1217.
- Nwogu, O. (1993), Alternative Form of Boussinesq Equations for Near-shore Wave Propagation, *J. Waterway Port Coastal Ocean Eng.*, *119*, 618–638.
- Oltman-Shay, J., P. A. Howd, and W. A. Birkemeier (1992), Shear instabilities of the mean longshore current: 2. Field data, *J. Geophys. Res.*, *94*, 18,031–18,042.
- Özkan-Haller, H. T., and Y. Li (2003), Effects of wave-current interaction on shear instabilities of longshore currents, *J. Geophys. Res.*, *108*(C5), 3139, doi:10.1029/2001JC001287.
- Pearson, J. M., I. Guymer, L. E. Coates, and J. R. West (1997), Mixing Processes due to breaking wave activity in the coastal zone, *Proc. Coastal Dyn.*, *97*, 197–206.
- Peregrine, D. (1998), Surf zone currents, *Theoret. Comp. Fluid Dyn. J.*, *10*, 209–295.
- Reniers, A. J., and J. A. Battjes (1997), A laboratory study of longshore currents over barred and non-barred beaches, *Coastal Eng.*, *30*, 1–22.
- Ruessink, B. G., J. R. Miles, F. Feddersen, R. T. Guza, and S. Elgar (2001), Modeling the alongshore current on barred beaches, *J. Geophys. Res.*, *106*, 22,451–22,463.
- Schäffer, H. A., P. A. Madsen, and R. Deigaard (1993), A Boussinesq model for waves breaking in shallow water, *Coastal Eng.*, *20*, 185–202.
- Schiff, K. C., M. J. Allen, E. Y. Zeng, and S. M. Bay (2000), Southern California, *Mar. Pollut. Bull.*, *41*, 76–93.
- Schmidt, W. E., B. T. Woodward, K. S. Millikan, R. T. Guza, B. Raubenheimer, and S. Elgar (2003), A GPS-tracked surfzone drifter, *J. Atmos. Oceanic Technol.*, *27*, 1069–1075.
- Slinn, D. N., J. S. Allen, and R. A. Holman (2000), Alongshore currents over variable beach topography, *J. Geophys. Res.*, *105*, 16,971–16,998.
- Spydell, M., F. Feddersen, R. T. Guza, and W. Schmidt (2007), Observing surfzone dispersion with drifters, *J. Phys. Oceanogr.*, in press.
- Tennekes, H. and J. L. Lumley (1972), *A First Course in Turbulence*, MIT Press, Cambridge, Mass.
- Thornton, E. B., and R. T. Guza (1986), Surf zone longshore currents and random waves: Field data and models, *J. Phys. Oceanogr.*, *16*, 1165–1178.
- Ting, F. C. K., and J. T. Kirby (1994), Observations of undertow and turbulence in a laboratory surfzone, *Coastal Eng.*, *24*, 51–80.
- Wei, G., J. T. Kirby, and A. Sinha (1999), Generation of waves in Boussinesq models using a source function method, *Coastal Eng.*, *36*, 271–299.
- Zelt, J. A. (1991), The run-up of nonbreaking and breaking solitary waves, *Coastal Eng.*, *15*, 205–246.

F. Feddersen, Integrative Oceanography Division, Scripps Institution of Oceanography, University of California, San Diego, La Jolla, CA 92093-0209, USA. (falk@coast.ucsd.edu)